BJR https://doi.org/10.1259/bjr.20191004

Received: 01 December 2019 | Revised: 16 October 2020 | Accepted: 26 October 2020

Cite this article as:
Gwilliam MN, Collins DJ, Leach MO, Orton MR. Quantifying MRI T_1 relaxation in flowing blood: implications for arterial input function measurement in DCE-MRI. *Br J Radiol* 2021; **94**: 20191004.

FULL PAPER

Quantifying MRI T_1 relaxation in flowing blood: implications for arterial input function measurement in DCE-MRI

MATTHEW N GWILLIAM, PhD, DAVID J COLLINS, BA, MInstP, MARTIN O LEACH, PhD, FInstP, FMedSci and MATTHEW R ORTON, PhD

CRUK Cancer Imaging Centre, Institute of Cancer Research and Royal Marsden NHS Trust, London, UK

Address correspondence to: Dr Matthew N Gwilliam
E-mail: *matt.n.gwilliam@gmail.com*

Objectives: To investigate the feasibility of accurately quantifying the concentration of MRI contrast agent in flowing blood by measuring its T1 in a large vessel. Such measures are often used to obtain patient-specific arterial input functions for the accurate fitting of pharmacokinetic models to dynamic contrast enhanced MRI data. Flow is known to produce errors with this technique, but these have so far been poorly quantified and characterised in the context of pulsatile flow with a rapidly changing T1 as would be expected *in vivo*.
Methods: A phantom was developed which used a mechanical pump to pass fluid at physiologically relevant rates. Measurements of T_1 were made using high temporal resolution gradient recalled sequences suitable for DCE-MRI of both constant and pulsatile flow. These measures were used to validate a virtual phantom that was then used to simulate the expected errors in the measurement of an AIF *in vivo*.
Results: The relationship between measured T1 values and flow velocity was found to be non-linear. The subsequent error in quantification of contrast agent concentration in a measured AIF was shown.
Conclusions: The T1 measurement of flowing blood using standard DCE- MRI sequences are subject to large measurement errors which are non-linear in relation to flow velocity.
Advances in knowledge: This work qualitatively and quantitatively demonstrates the difficulties of accurately measuring the T1 of flowing blood using DCE-MRI over a wide range of physiologically realistic flow velocities and pulsatilities. Sources of error are identified and proposals made to reduce these.

INTRODUCTION

Dynamic-contrast-enhanced (DCE) MRI is widely used in order to assess vascular function, and has received much recent attention in clinical oncology trials of vascular targeted agents, amongst other applications.[1,2] DCE-MRI is used to measure the uptake of an injected contrast agent over several minutes in a tumour, and appropriate modelling of these data can yield quantitative measures of clinically informative vascular properties.[3,4]

In order to compute such measures of vascular function an arterial input function (AIF) is required. The AIF describes the concentration of contrast agent in the vascular space as a function of time. Ideally this would be measured for each visit in each patient to account for the natural variations in the AIF which have been observed in adults,[5] and are particularly pronounced in paediatric subjects.[6] An accurate measurement method for the concentration of contrast agent is, therefore, desirable but has proven challenging in practice. The use of a population-averaged AIF has been suggested[7] but variations in patient AIF between visits will be erroneously propagated to changes in the tissue vascular parameters.[8] Despite this, comparisons of the repeatability and sensitivity to treatment effects obtained using population and individually measured AIFs have shown that in practice using a population-averaged AIF gives better repeatability and comparable treatment sensitivity to individually measured AIFs.[9] This result was obtained using data acquired with a spoiled gradient echo sequence, and it implies that AIF measurement errors obtained with this widely used sequence are on average larger than natural variations in the AIF. More recently, a functional form of a population AIF which retains the characteristics of an individualised AIF has been described but the measurement of a patient-specific AIF remains sought after.[10]

An obvious way to obtain a patient-specific AIF is to monitor a blood vessel in the imaging volume.[11–15]

However, in order to ensure observable uptake in the tissues of interest, the concentration of contrast agent in the feeding blood vessels is so high that it cannot be measured accurately, *i.e.* the relationship between high concentrations of contrast agent and signal is non-linear. To avoid this, a pre-bolus experiment[16,17] has been proposed and pursued by many in the field whereby a 1/10th dose of contrast agent is delivered prior to the main examination. The observed contrast agent concentration is then scaled to approximate the AIF during the main examination.

However, imaging flowing blood remains challenging, and this is especially true for the spoiled gradient echo sequences that are widely used for DCE-MRI acquisitions. Where quantitative contrast agent concentration measures are required, T_1 quantification of the spoiled gradient echo signal must be performed, which means that the MR signal must be in a steady state.[18,19] In tissues, the contrast agent dynamics are such that the steady state assumption applies with good accuracy, but this may not be true for the flow velocities observed in blood vessels typically used for measuring AIFs. This is because the blood entering the field of view during the volume excitation delivers spins that have been subject to insufficient excitations to reach a steady state. In addition, blood flow in major arteries is highly pulsatile, which further complicates the measurement.

Techniques that use the phase of the imaging signal to measure the AIF[20–23] avoid many of the difficulties associated with inflow effects. However, the phase of the signal has lower precision due to reduced signal-to-noise. *Foltz et al,*[24] compares phase and magnitude methods and additionally notes that phase information is not readily available on most imaging units meaning that phase methods are not easily accessible to many users. Hence, this paper focusses on the magnitude methods which are more widely available.

Existing work using the magnitude signal has largely been limited to static phantoms with analytical models[25] or with constant flow rates such as *Roberts et al, 2011*.[26] Experiments were conducted by *van Schie et al, 2018*,[27] using a low (in the context of that seen in major arteries), constant flow velocity and a method to potentially correct these errors was proposed. *Garpebring et al, 2011*,[28] used a phantom with a Gaussian-like flow velocity waveform to examine the effects of inflow and non-ideal RF spoiling and made several recommendations, including orientating the images in parallel with the main B_0-field, but confirmed the that flow effects remain an obstacle. Rather than correct the imaging signal, *Han et al, 2011*,[29] proposed deliberately exciting spins before entering the imaging volume to reduce the signal error; work which was validated using a low velocity pulsatile phantom. A phantom that used relatively low velocity but pulsatile flow is described in the aforementioned work by *Foltz et al 2019*,[24] and was used to compare measurements of the passage of a bolus of contrast agent using both phase and magnitude-based DCE-MRI and DCE-CT. *Ning et al, 2018*,[30] has applied and expanded much of this work in animal models to demonstrate improvements in the repeatability of pharmacokinetic modelling.

What is missing from the literature, which would help guide future directions in this area, is a empirical characterisation of the measurement error introduced by flow across the entire range of flow velocities seen in major human arteries. Furthermore, the impact of physiologically realistic pulsatile flow seen over the course of the cardiac cycle needs to be understood. The work presented here (1) examines the impact of flow on T_1 quantification across the range of physiologically realistic flow rates, (2) directly assesses the effect of *pulsatile* flow, similar to that seen in the major arteries that are commonly used to measure arterial input functions, and (3) uses a validated virtual phantom to examine the likely errors that would be seen *in vivo* with pulsatile flow during the passage of a contrast agent causing rapidly changing T_1.

METHODS AND MATERIALS

The aim of this work is to not only quantify the measurement error introduced by flow on quantitative imaging of T_1, but to assess the implication of these errors within the context of measurement of an AIF for DCE-MRI. Specifically, the suggestion of a prebolus experiment whereby the T_1 of blood in a major artery is dynamically measured is explored. Assessing the implications of these errors is further complicated as the T_1 of the blood is rapidly changing. This study uses a physical phantom in order to accurately reproduce a range of both constant and physiologically realistic pulsatile waveforms in a tube of similar diameter to a large artery such as the carotid or femoral. These arteries usually run in parallel with the main B_0-field and physical phantom design and subsequent image orientations were chosen to mimic this (and follow the recommendations in *Garpebring et al,2011*[28]). Although the imaging signal, and subsequent T_1 measurement is expected to vary across the image space, *i.e.* be more accurate at more efferent locations, to maximise signal and reduce noise, we focus on a section of the image space at the centre of the physical phantom, which is in the middle of the coil. This approach enables us to validate the virtual phantom, which can be used to describe errors in different locations and with different imaging parameters. However, *in vivo* the T_1 of the pulsatile blood flow is also changing as the bolus of contrast agent passes. This is very difficult to repeatedly simulate with a physical phantom. Hence, the results from the physical phantom with a constant underlying T_1 were used to validate a virtual phantom whose underlying T_1 could be easily changed to simulate those expected in a pre-bolus experiment.

This section first describes the construction and set up of the physical phantom, the flow waveforms produced by the phantom, and the methodology used to establish a baseline T_1 measurement of the blood-mimicking fluid (BMF). Then, the imaging sequences and image processing methodologies are defined, these being designed to replicate clinically feasible practices whilst isolating the errors introduced by flow.

Finally, the design of the virtual phantom is discussed and its use described.

Physical phantom

The physical phantom was designed to reproduce the scenario of blood flowing through a major artery in a patient. A tube of similar

Figure 1. Room diagram showing the flow phantom, pump unit and control PC, and closed loop of ~6 m of plastic tubing,~70 cm of which was 19 mm inner diameter pipe.

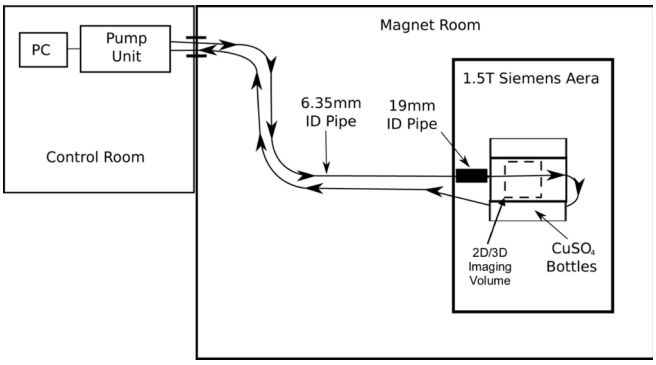

diameter to that of a major artery was chosen and attached to a pump capable of delivering both continuous flow velocities and pulsatile waveforms similar to those seen *in vivo*[31,32] . The practicalities of building such a phantom in a clinical imaging centre placed a number of constraints on the design and these will be discussed below. A diagram of the experimental setup is shown in Figure 1. An MR compatible, programmable syringe pump[33] was used to generate either constant flow or a repeated pulsatile waveform in a closed loop of tubing containing the manufacturer supplied and required BMF consisting of a 4:5 mix of glycerol and water which has a similar viscosity to blood. The pump was controlled by a PC, and both were sited outside the magnet room with the connecting tubes passing through a waveguide. A 6m long length of flexible plastic tubing (6.35 mm internal diameter, similar to the femoral artery) formed a closed loop between the input and output ports of the programmable pump. A section of the tubing was held straight inside a short length of rigid Perspex tubing which passed between three loading bottles containing $CuSO_4$ solution (1 litre each, consisting of 770 mg $CuSO_4$, 1 ml arquad (1%), 0.15 ml H_2SO_4, in 23 cm tall, 9.5 cm diameter plastic bottles) placed inside the head coil at the isocentre of the imaging unit (Figure 2).

Figure 2. Diagram shows an axial cross-section of the experimental setup, indicating the components of the flow phantom inside the head coil. The 3D imaging volume is shown and the phantom is imaged so that coronal images are obtained. The Perspex sheath separates the tubing from the edge of the $CuSO_4$ bottles ensuring there is enough gap to enable a 3D/2D ROI to be defined that only includes signal from the BMF.

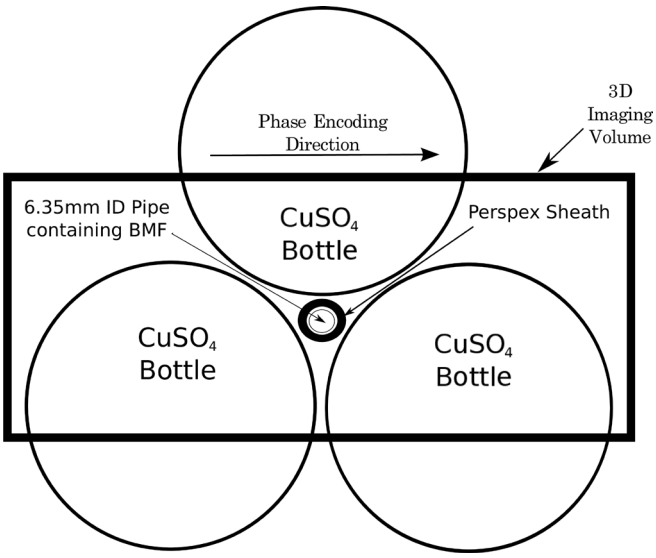

In vivo, the blood flowing into the imaging volume in a major artery has recently passed through the heart twice and traversed the lungs. Therefore, it is assumed that it has been in the main B_0-field of the magnet for a long length of time relative to its T_1 and enters the imaging volume close to fully polarised. Its spin history outside the imaging volume is difficult to know but it is expected that it will have received some excitations from the B_1 field, but not enough to have reached saturation. In contrast, the fluid entering the imaging volume in the physical phantom will have flowed from the pump outside the imaging room. To more closely replicate the B_0 and B_1 fields that blood in a patient experiences, an early iteration of the physical phantom had a coil of pipe at the centre of the magnet through which the BMF flowed before entering the imaging volume. However, such a long length of pipe of this diameter (6.35 mm) generated such resistance to flow that the pump was unusable. Therefore, the long coil of pipe was replaced with a short length of wider diameter pipe (19 mm), allowing the pump to run up to 100 $cm.s^{-1}$ in the 6.35mm pipe where measurements are made, and reducing the flow velocity in the 19mm diameter section of pipe. In terms of the magnetic field history of the BMF, the 19 mm pipe can be thought of as simulating the passage of the blood through the lungs and heart before entering the imaging volume, *i.e.* experiencing the B_0 field but outside the imaging volume. It is calculated that the BMF experienced greater than 4 x T_1 periods before being imaged.

The continuous flow velocities tested were chosen to span the physiological range of instantaneous flow velocities seen in major arteries:[31] 0, 3, 6, 9, 13, 16, 32, 47, 63, 79, 95 $cm.s^{-1}$ (unfortunately the image data for the four higher velocities were lost for the 2D sequence). Figure 3 shows the pre-programmed flow waveforms used in this study which are representative of those seen in humans in the femoral (red) and carotid (blue) arteries. The mean flow velocity of these waveforms being 31 and 12% of the peak velocities over the cycle - it is the mean flow velocity which is reported in the results from pulsatile flow. The mean flow velocities of these pulsatile waveforms were chosen to be the same as those used above for continuous flow velocities.

Establishing the T_1 of static BMF

Images were obtained using a Siemens Magnetom Aera 1.5 T. Baseline T_1 measurements of the BMF were obtained using an inversion recovery sequence at 1.5 T with the following parameters: TR: 10000 ms, TE: 1.2 ms, pixel size: 2.3 mm, FA: 6°, slice thickness: 8 mm, acquisition matrix: 128 × 128, bandwidth: 490 Hz/pixel, TI: 0, 131, 150, then 200–1300 in increments of 100, then 1500–4000 in increments of 500 ms.

Figure 3. Plot of physiological waveforms provided by the Compuflow 1000MR. Negative flow rate indicates reverse flow in the tubing.

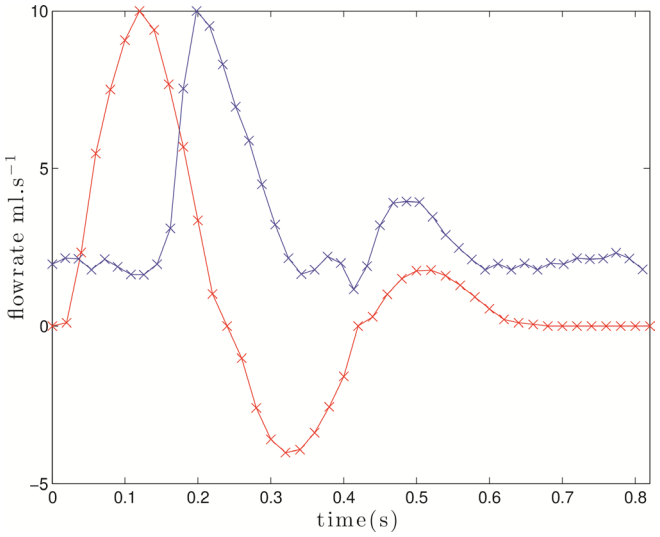

Spoiled gradient echo image acquisition

Two imaging protocols were chosen to be similar to those used in our institution: a 3D protocol for measuring contrast uptake in tissues,[34] and a 2D protocol used for pre-bolus AIF measurements in large vessels. In both cases coronal slices were used. Baseline estimates of T_{10} and M_0 (proton density-weighted image scaling) are obtained from the imaging signals at two flip angles using the method of *Fram*.[18] Assuming the M_0 scaling term is constant during the contrast-enhancement phase, dynamic measures of $T_1(t)$ are obtained from the dynamic images acquired using a single flip angle (18). Measurements of the T_1 of BMF were obtained over a range of constant and pulsatile flow velocities (discussed above).

The spoiled gradient echo imaging parameters for the 3D/2D protocol were TR = 3.0/5.5 ms, TE = 0.95/1.21 ms, 2.3 × 2.3 mm pixels, 108 × 128/128 × 128 matrix size, 248 × 294/294 × 294 mm field of view, slice thickness 5 mm, bandwidth 650/1395 Hz/

Figure 4. Coronal images were converted into axial slices. The coronal images on the left depict signal from the pipe running along the z axis. The central axial slice intersects the centre of the pipe, hence the widest area of signal (grey). The slice immediately below and above the central slice intersect a smaller cross-section of the pipe and so have narrower columns of signal. The top and bottom image do not intersect with the pipe at all. Reformatting the slices this way enabled a ROI to be drawn to isolate the signal from the pipe.

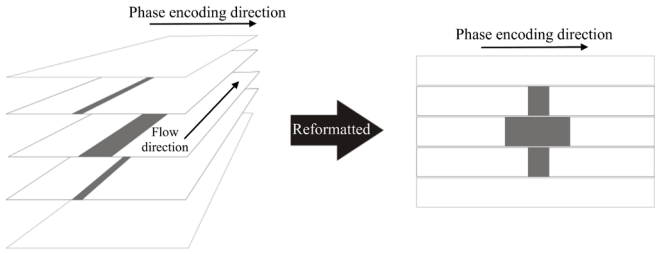

Pixel, and GRAPPA factor of 2. The flip angles were 3.5° and 7° for the 3D sequence and 5° and 10° for the 2D sequence, and these were chosen to bracket the Ernst angle (*Wang et al 1987*,[35] *Imran et al 1999*[36]) for the T_1 of the BMF (found in section 2.2) and TRs used for each sequence - the Ernst angles were 4.9° for the 3D and 6.7° for the 2D sequences. The 3D sequence consisted of 14 coronal slices per volume acquired in 2.9 s, and 10 low flip angle pre-contrast followed by 50 high flip angle volumes were acquired dynamically for each flow scenario. The 2D sequence used a single coronal slice (the central slice in Figure 4 acquired in 0.7 s and 50 low flip angle pre contrast images followed by 50 high flip angle dynamic images were obtained).

Image processing

All image analysis and simulations were conducted using MATLAB (The Mathworks, Natick, MA). A cylindrical (3D) or rectangular (2D) volume of interest (VOI) was constructed for both the 2D and 3D images to select voxels that are inside the straight section of tubing and within ±10 mm of the centre of the (coronal) image plane along the axis of the tubing. This was trivial for the 2D sequence images. For the 3D sequence, the image volume was axially reformatted and circular regions of interest (ROI) were drawn inside the cross-section of the tubing on the reformatted slices (Figure 4). This was done on each reformatted slice that corresponded to the ±10 mm extent defined above.

For each experimental condition a single signal value for the low flip-angle images was obtained by averaging over the VOIs, then averaging these over the repeated acquisitions (as required by the Fram method, initial images not in a steady-state were excluded – either one or three images for the 3D and 2D sequences respectively). The average signals from the VOI were then obtained for each of the dynamic images. Dynamic T_1 estimates for each experimental condition were produced using the Fram equation:

$$T_{1-True} = -\mathrm{TR}.\left(\log\left(\frac{S_2}{\sin(\theta_2)} - \frac{S_1}{\sin(\theta_1)}\right)\right)^{-1} \quad (1)$$

(1) where $\theta_{1/2}$ are the low and high flip-angles (LFA, HFA) and $S_{1/2}$ are the corresponding measured signals.

Flip angle correction

The flip angle a spin experiences is a function of the B_1 field. As the B_1 field is not homogeneous in practice, the flip angle a spin experiences varies from the user defined value.[37] This error will be propagated through the Fram equation leading to an inaccurate measurement of T_1. As the aim of this work was to investigate errors introduced by flow, the true flip angle experienced by every spin was estimated, as follows, to allow for more accurate T_1 estimation using the Fram method. Firstly an inversion recovery sequence using 19 inversion times between 0 and 4000 ms was used to establish the T_1 of static BMF (see section 2.2 - a method which is not susceptible to B_1 field inhomogeneities. Adapting equation 1 to include an inhomogeneity factor f we have:

$$T_{1-True} = -\mathrm{TR}.\left(\log\left(\frac{S_2}{\sin(f\theta_2)} - \frac{S_1}{\sin(f\theta_1)}\right)\right)^{-1} \quad (2)$$

Figure 5. Flip angle correction factor profiles for the 3D and 2D sequences assuming a T_1 of 812 ms. The direction of flow in this work is in the z-direction.

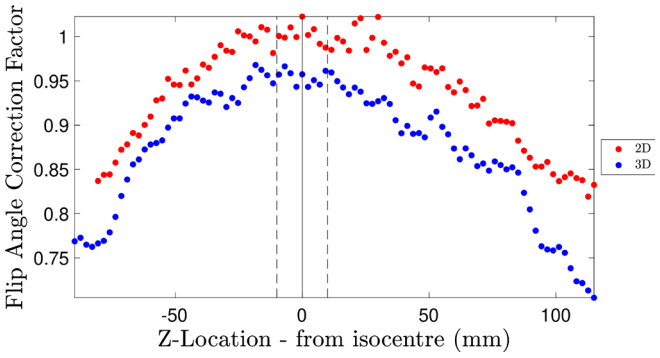

By acquiring the spoiled gradient echo sequences discussed in section 2.3, S_1 and S_2 are measured which allows equation 2 to be solved for f. The true flip angle for each spin is found as $\theta_{1/2}$, $True = f\theta_{1/2}$.

Virtual phantom

A simulation was performed in MATLAB which used the following equation derived from the Bloch equations[19], to simulate signals from a sequence with the same parameters as above:

$$S(\alpha) = -M_0 \sin\alpha \left(\frac{(1-E_1)(1-\cos\alpha.E1)^n}{1-\cos\alpha.E1} + (\cos\alpha.E1)^n \right) \quad (3)$$

where α is the flip-angle, $E_1 = e^{\frac{-TR}{T_1}}$ and M_0 is the equilibrium magnetisation. The aim was to assess the error that flow introduces when quantifying T_1 with a double flip angle acquisition due to incomplete saturation of the signal. Given the time between excitations and the flow velocity, and assuming a spin would experience no excitations before entering the image volume, the number of excitations the spin would have experienced at each point in the imaging volume is governed by: n = distance into imaging volume of voxel/(TR × velocity). Assuming a constant magnetic field whilst in the image volume, the above equation was used to calculate the simulated signal for each spin in the virtual imaging volume.

Using equation 1, estimates of T_1 were generated from the simulated signals from the virtual phantom using the same flip-angles as used in the physical phantom. As with the physical phantom, the sum of the signal across 20 mm at isocentre was used. The results from the physical phantom were used to verify the accuracy of the virtual phantom.

The virtual phantom allowed the measurement error to be assessed over a range of imaging parameters, underlying blood T_1 and velocities.

The virtual phantom was also used to simulate the measurement of flowing blood T_1 across a range of physiologically realistic flow velocities with the same imaging parameters used with the physical phantom.

Simulated pre-bolus measurement

The measurement of an AIF involves the dynamic T_1 measurement of blood which has a rapidly changing T_1 as the contrast agent bolus moves although the imaging volume. To simulate this, a mean Parker population AIF[7] scaled by 1/10th is used to simulate the dynamic underlying T_1 of blood during a pre-bolus experiment assuming a pre-contrast agent T_1 value of blood to be a physiologically realistic 1480 ms[38]. Using these T_1 values, the virtual phantom was used to find the maximum and minimum measured concentration of contrast agent as the flow velocity is varied from 0 to 75 cm.s^{-1} (a range which spans the bulk of the velocities expected in the aorta) measured 15 cm into the imaging volume. The same sequence described in section above was simulated. To give an insight into how sensitive the measurement of T_1 may be across the normal range of population AIFs and at commonly used flip angles, simulations were repeated using the mean Parker population AIFs ± 1 standard deviation and at flip angles of 3.5°/7° and 3°/16°. The aim of this analysis was to provide an estimate for the range of likely error *in vivo*.

RESULTS

The T_1 of BMF

The results of the IR experiment indicated that the BMF had a T_1 of 812 ms which was used as the true value of the BMF in further analysis.

Flip angle correction

The calculated correction factor for each voxel along the length of the tube is shown in Figure 5.

T_1 quantification using spoiled gradient echo sequences

The results of measuring the T_1 of static BMF with the physical phantom are shown in Table 1, for constant flowing BMF in Figure 6 and Table 2, and for pulsatile flow in Figure 7.

Virtual spoiled gradient echo signal and flow

The signal produced from BMF entering the virtual phantom as it flows into the imaging volume is shown in Figure 8 for both low and high flip angle simulated sequences. The corresponding T_1 values estimated from these signals using equation 1 are also shown.

T_1 measurement flow response using a spoiled gradient echo sequence with the physical and virtual phantoms

Figure 6 shows that the T_1 estimated using the Fram method has a non-linear relationship with the flow velocity in the physical phantom when measured with 2D and 3D sequences (solid lines). This relationship is also replicated with the virtual phantom (dashed) although the peak of the overestimate is shifted to a higher flow velocity. The error introduced by flow became statistically significant ($p = 0.05$) at 3.7 cm.s^{-1} for 3D and 17.7 *cm.s*$^{-1}$ for 2D.

When the flow is pulsatile, the results from the physical phantom show that the measured T_1 varies with the mean flow

Table 1. Table comparing the measured T1 from the 2D and 3D sequences for static BMF. The error is based on a value of 812 ms obtained in section 3.1, and the standard deviation is computed from all voxels inside the tubing VOI

Sequence	Mean T_1 over 20 mm region at isocentre (ms)	Standard deviation (ms)	% difference from baseline
2D	816	17	0.5
3D	739	13	9.0

velocity (Figure 7). Pulsatile flow increases the standard deviation of the measures with the more pulsatile femoral waveform causing greater measurement variance than the carotid. The flow velocities stated are the mean velocities produced by the waveforms, *i.e.* 31% and 12% of peak flow velocity for the carotid and femoral waveforms respectively. The increased variance is particularly prominent with the 2D sequence. Despite the increased variance, the mean measures from the pulsatile flows show a similar pattern to the constant flow velocities.

The virtual phantom was used to simulate the measured T_1 of a range of underlying T_1s. The contours in Figure 9 join lines of equal measured T_1. For example, the results show that a measured T_1 of 1500 ms (Figure 9, yellow) could represent an underlying T_1 of between 1100 ms and 1600 ms for flow velocities between 0 cm s^{-1} and 60 cm s^{-1}.

Figure 6. Plots showing mean measured T_1 of BMF at various constant flow velocities. The error bars indicate one standard deviation over 50 images.

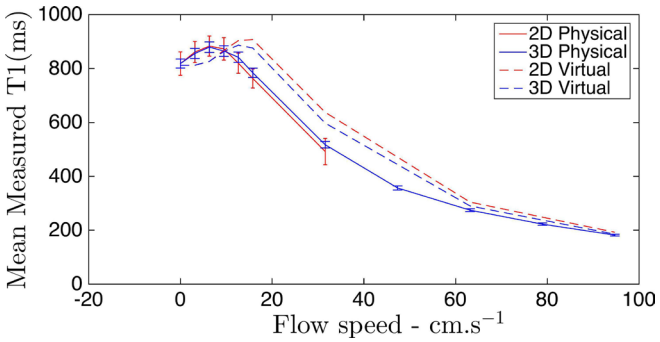

Simulated pre-bolus measurement

To demonstrate the effect of flow related bias on the AIF curve, a Parker population AIF scaled by $1/10^{th}$ was used to simulate a pre-bolus experiment[16,17], see Figure 10. Error bars indicate the range of values obtained using the virtual phantom at four key time points for constant flow velocities between 0 cm s^{-1} and 75 cm s^{-1}, which are similar to those found in the aorta.

DISCUSSION

It has been shown that accurate measures of contrast agent concentration are desirable for the fitting of models to uptake curves.[3,39] Various workers measure the passage of a bolus of MRI contrast agent using spoiled gradient echo sequences in order to obtain an AIF for model fitting. This work assesses the error due to flow that exists in these measures. By quantifying and describing the sources of error, we inform the discussion around the strategies being employed as the field strives towards more accurate quantitative measures of vascular function.

It is accepted within the community that current techniques are sensitive to treatment in the context of whole-trial analyses. However, uncertainty in the measurement of the AIF undermines the interpretation of models which purport to be

Table 2. Measurement error as a function of constant velocity for the 3D and 2D sequences

	3D		2D	
Constant flow velocity (cm s^{-1})	% difference from baseline	Standard deviation (ms)	% difference from baseline	Standard deviation (ms)
0	0	17	0	43
3.2	3.7	17	4.9	39
6.3	5.6	19	7.7	37
9.5	5.9	20	6.5	41
12.6	1.6	19	0.1	35
15.8	−5.7	18		
31.6	−37.3	12		
47.4	−56.7	7		
78.9	−72.8	4		
94.7	−77.6	3		

Figure 7. Plots showing the mean and standard deviation of T_1 over 50 measurements as a function of the mean flow velocity (over cardiac cycle) for pulsatile waveforms, 3D (upper) and 2D (lower). Mean flow velocity seen in an adult male is around 30 cm s^{-1} in the carotid artery and around 10 cm s^{-1} in the femoral artery. True T_1 is 812 ms.

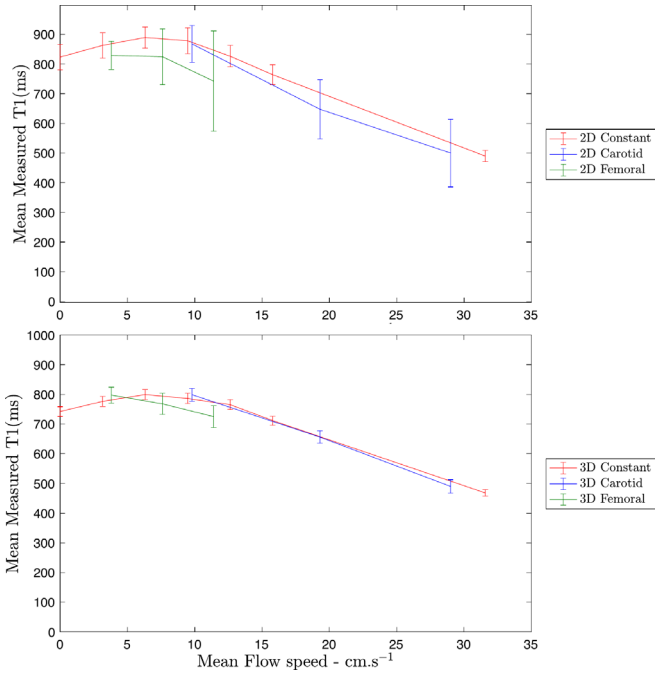

Figure 8. Plot of simulated low (red) and high (blue) flip angle signals obtained from flowing virtual BMF. LFA/HFA = 3.5°/7°, TR = 3 ms and flow velocity = 5 cm s^{-1}. The signals are used to create the T_1 curve via the Fram equation are shown in green. The BMF produces high signal as it arrives in the imaging volume (left) and reduces to a steady state as it recieves more excitations and passes through the volume. The HFA signal for the BMF is higher than the LFA signal when it first enters the imaging volume but reaches a steady-state below the signal from the LFA sequence. The differing behaviours of these signals as they approach a steady state results in the non-linear measured T_1 shown. "True" T_1 is 1200 ms.

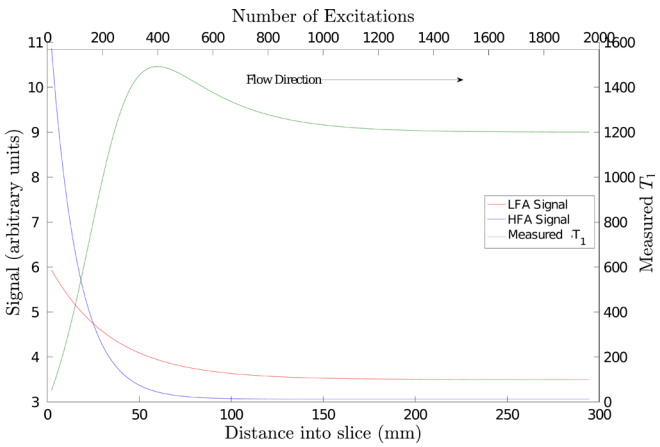

Figure 9. Contour plots of measured T_1 for a range of T_1 and flow velocities simulated using flip angles of 3.5° and 7°(top), and 3° and 16° (bottom), with a TR of 3 ms. The contours join points of the same measured T_1.

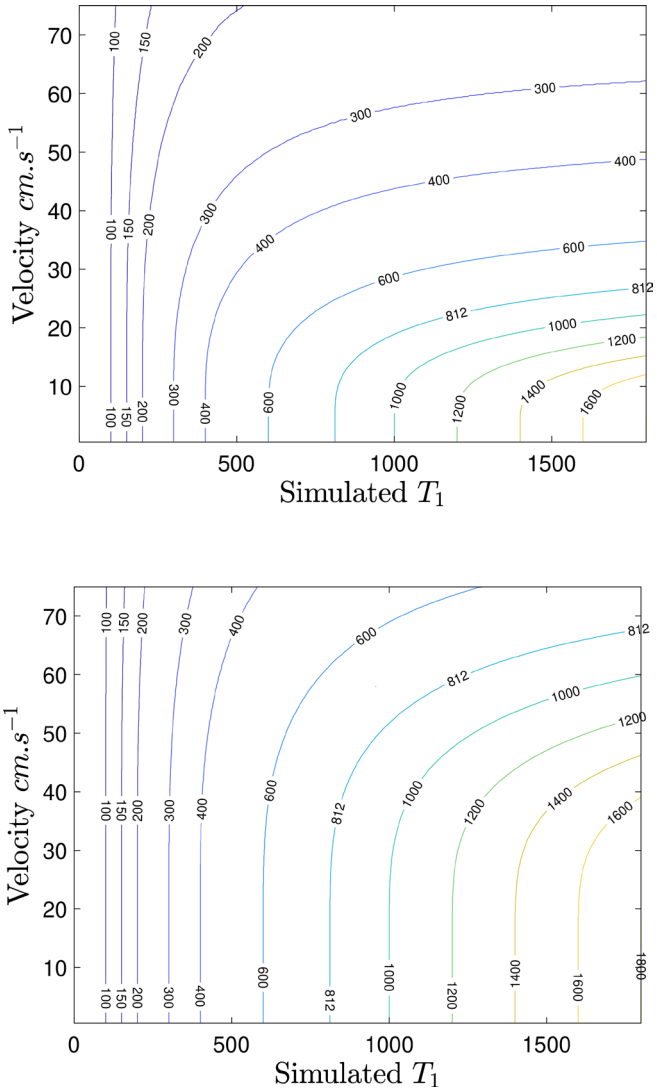

quantifying sought-after measures of vascular function on an examination-by-examination or even pixel-by-pixel basis.

Following the order of the results, this section discusses the impact of using flip angle correction to isolate the error introduced by flow, the quantification of T_1 using the physical phantom and how these measures were used to validate the virtual phantom. Finally, a summary of the implications for those working in the field of DCE-MRI is discussed.

Flip angle correction

The type of flip angle correction profiles seen in Figure 5 for the coronal plane are entirely consistent with those shown in previous work[37,40] The correction factor profiles assume that all of the error in T_1 quantification is because of an inhomogeneous B_1 field. The error on the absolute measurement observed here should be noted for future studies using the double-flip angle

Figure 10. Graph showing a simulated pre-bolus AIF (blue), *i.e* a typical Parker population AIF at 1/10th dose - the blue error bars indicate the population standard deviation. (courtesy of G. Parker). The virtual phantom is used to find the maximum and minimum gadolinium concentration that would be measured as the flow rate is varied from 0 to 75 cm s^{-1} at key points as the bolus passes. The simulated measures are offset for clarity. The simulated measures are also obtained for a Parker population functions ± 1 standard deviation. It is clear that the bolus with a larger peak (+1 standard deviation) is less susceptible to flow induced measurement errors. It is also clear how sensitive the measures are to choice of flip angles.

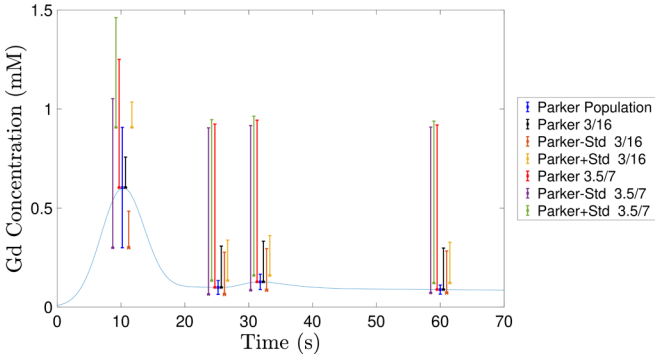

method. It seems likely that this error is due to spins away from the centre of the imaging volume being nutated through angle less than the prescribed flip angle.

T_1 quantification using spoiled gradient echo sequences

There is increased standard deviation in the measurement of T_1 with the 2D sequence compared to the 3D (Figures 6 and 7). This is likely due to the reduced signal to noise due to its decreased measurement volume and image acquisition time.

Virtual spoiled gradient echo signal and flow

The non-linear relationship between flow velocity and measured T_1 can be explained using Figure 8, which describes the relationship between the measured imaging signals and distance into the imaging volume for a constant flow velocity using the virtual phantom; *i.e*. how the signals change as they experience more excitations. As the spins travel further into the imaging volume (from left to right), they are subject to more excitations and each curve monotonically reaches its steady-state at a rate that depends on the sequence flip- angle. If the flow velocity is increased, the number of excitations experienced when the spins have reached isocentre will be reduced, i.e. the curves in Figure 8 will be stretched along the x-axis away from the origin. The Fram method (equation 1) produces a measurement of T_1 from a function of the low and high flip angle image signals and as shown in Figure 8, the high flip angle signal initially has a higher signal magnitude than the low flip angle signal, but reaches a lower magnitude at steady state. This results in the T_1 measurement rising and then overshooting the correct measurement, before falling to the correct value as the distance into the slice increases.

T_1 measurement of non-pulsatile flow using a spoiled gradient echo sequence with the physical and virtual phantoms

The non-linear relationship between flow velocity and T_1 measurement in the physical phantom is qualitatively replicated by the virtual phantom, but the curves in Figure 6 for the virtual phantom are shifted to the right. It is hypothesised that this discrepancy is due to the virtual phantom simulating a perfectly homogeneous RF excitation profile across the imaging volume. The actual excitation profile experienced by the physical phantom is influenced by a variety of factors such as B_1 and slice profile variations. Importantly, excitations of unknown nutation angle affect the BMF before it enters the imaging volume. Therefore, the spin history of the magnetisation at isocentre is different to that simulated by the virtual phantom. None of these factors are easily mitigated, especially within the clinical context. A subject in the scanner will have nearly all their blood within the main B_0-field and close to the imaging volume, thus it will be equally difficult to characterise the spin-history of blood before it enters the imaging volume.

AIF measurement

There are large uncertainties in the measurement of T_1 due to flow. These errors are non-linearly related to flow across the range of mean velocities seen in large vessels. These difficulties are further exacerbated by pulsatile flow and in the case of fast 2D imaging due to the temporal variation in mean velocity during a signal acquisition. Flow pulsatility would be difficult to model in practice and subsequent changes in measured T_1 are largely treated, incorrectly, as part of the "noise". However, the observed increased variance introduced by pulsatile versus constant flow was not large when using the 3D sequence. It may be possible to partially correct the measures from a slower imaging sequence if the mean flow velocity is known. However, for faster imaging sequences, the mean flow velocity over each individual image acquisition would be required.

In practice a bolus injection of contrast agent is used. While the rate of change of contrast during the equilibrium Phase is negligible compared to the effects of pulsatile flow, the same is not true during the initial passage of the bolus in the major vessels (around 10–15 sec). The random interaction between the change in T_1 due to changes in contrast agent concentration and the T_1 measurement error introduced by pulsatile flow further complicates the accurate measurement of T_1.

Figure 10 shows the errors introduced by flow and the sensitivity of the errors to flip angle. This should be considered when designing sequences. The sequence with the 3° and 16° flip angles is less susceptible to flow induced measurement errors than the 3.5° and 7° flip angle measures. Additionally, the variation in experienced flip angles across the imaging volume (Figure 5) should also be considered - these variations may impact attempts at correcting flow affected signals.

Pre-bolus measurement

For a fixed T_1, the T_1 that will be measured varies as a function of flow velocity. Thus, pulsatile flow will yield a range of measured

T_1, *e.g.* for a typical blood T_1 of 1500ms, the range of T_1 that is measured varies non-linearly from 1500ms to ~1130 ms as the flow velocity is increased from 0 $cm.s^{-1}$ to the relatively low velocity of 50 $cm.s^{-1}$ (Figure 9). The introduction of the contrast agent will reduce the true T_1 making measurement accuracy less susceptible to flow. If the underlying T_1 of blood were lower to begin with, the plots on Figure 9 show that less measurement variability would be introduced by flow. For example, the range of T_1 that would be measured if the underlying T_1 were 900 ms would vary non-linearly from 900 ms to ~766 ms as the flow velocity is increased from 0 $cm.s^{-1}$ to ~50 $cm.s^{-1}$.

When using a separate acquisition to measure the AIF (such as the already discussed pre-bolus experiment), less error would be introduced by flow if it were performed after the main DCE-MRI acquisition since the contrast agent-administered for the main DCE-MRI examination will be well mixed in the blood, thereby reducing its baseline T_1. This may be particularly useful in avoiding bias in the establishment of the baseline T_{10}. However, in this scenario, the decrease in the T_1 of blood prior to the AIF measurement will mean a smaller contrast between this signal and the subsequent peak signal, leading to a greater uncertainty in the T_1 measures. Further investigation is required to assess whether measuring the AIF in this way would be worthwhile.

Summary and implications for those working in DCE-MRI

This paper assesses the expected inaccuracy in T_1 measurement due to physiologically realistic pulsatile flow using a physical phantom which is used to validate a virtual phantom. Results from both phantoms inform the discussion and should be of interest to those working in DCE-MRI and particularly those looking to use model fitting to obtain quantitative measures. We expand on previous work, particularly by *Roberts et al.*[26] and more recently by *van Schie et al.*[27] , by examining flow velocities and pulsatilities which are similar to those observed *in vivo*.

The effect of flow on T_1 measurement using the double flip angle method

The effects of flow on T_1 measurement are large compared to the changes which would be observed during the passage of a bolus of contrast agent and are non-linear with flow velocity. ROIs used for measuring AIFs should be placed as far away as possible from the entry points of flow to the imaging volume to reduce this effect.

Model fitting

The ability to obtain absolute quantitative measures of vascular function by fitting models to DCE-MRI data is questionable given that no strategy has yet been shown to accurately measure the AIF. Reporting of the absolute model parameter values which purport to be related to function, rather than changes from a baseline, should be discouraged.

Correcting the signal from flowing spins

If the mean flow velocity were known, *e.g.* through phase difference techniques,[41] it seems feasible to partially correct the T_1 measurements. *Peeters et al*[25] and *Van Schie, 2018*[27] proposed methods to do this by obtaining the number of excitations a flowing fluid has received at a point and then correcting for it. This work further illuminates difficulties in applying this technique *in vivo* given the large variations in T_1 measurement which pulsatile flow is shown to introduce. Such strategies would need to account for the range of excitations observed over the cardiac cycle. Arteries with lower pulsatility may present easier targets for potential correction of the inflow-effect. It may be that the use of complementary quantitative flow techniques may inform the choice of artery and could provide data, which would assist in the correction of the in-flow effect over the cardiac-cycle on a per-patient/examination basis. Given the large variation in pulsatilities and flow velocities observed across subjects,[32] along with the variance in the prior number of excitations that may be experienced by incoming blood as it passes through potentially tortuous feeding arteries near to the imaging volume, such corrections would need to be bespoke for a particular examination.

Sequence and examination design

Higher flip angles reach saturation more quickly, as the signal is a function of $cos(\alpha)^n$ (see equation 3), thus reducing the in-flow-effect. This should be a consideration during sequence design along with other factors discussed in *De Neayer et al, 2011*.[42] Measurement error due to the inflow effect may be reduced if the AIF is measured after the main DCE- MRI investigation (discussed above).

Alternative approaches to AIF measurement in a vessel

Even if measurement error could be reduced to zero, the measurement of AIF in a feeding vessel is still a proxy for the plasma curve in the tissue. Therefore, solving the inflow effect issue would not yield a perfect model fit. In the context of clinical trials, a population AIF has been shown to provide results where the repeatability is low enough that clinically useful changes can be measured.[9] Therefore, it is suggested that rather than pursuing further improvement to these techniques, *i.e.* towards more quantitative measures, more effort should be spent developing methods for tissue-level AIF estimation, similar to that of *Schabel et al, 2010*.[43] Reference tissue approaches are attractive in principle but their effectiveness in practice is contingent on the contrast dynamics of the two regions being complimentary, which cannot always be guaranteed.

Proposed radial acquisitions[44] have significant advantages over Cartesian imaging in terms of spatial and temporal resolution, and this work indicates that similar evaluations to assess the robustness of radial acquisitions to pulsatile flow should be undertaken.

CONCLUSION

Quantitative T_1 measurement using spoiled gradient echo sequences in blood is severely compromised by its flow. The relationship between measurement error and flow is highly non-linear which seems likely to complicate any attempt to correct this, especially given the pulsatility seen in arteries. Of particular note for DCE-MRI, these findings indicate that any AIF obtained for the fitting of pharmacokinetic models from monitoring the

T_1 of blood in an artery is likely to be inaccurate. Thus, the value of such strategies is undermined.

ACKNOWLEDGEMENTS

We acknowledge the support received from a Medical Research Council (MRC) Centenary Award, the Engineering and Physical Sciences Research Council (EPSRC) [EP/H046410/1], Cancer Research UK (CR-UK) Cancer Therape utics Unit [C309/A11566], CR-UK and EPSRC Cancer Imaging Centre, in association with the MRC and Department of Health (England) [C1060/A10334,C1060/A16464], and NHS funding to the NIHR Biomedical Research Centre and Clinical Research Facility at The Royal Marsden and the ICR. Professor Martin O Leach is an NIHR Emeritus Senior Investigator.

REFERENCES

1. Patterson DM, Rustin GJS. Vascular damaging agents. *Clin Oncol* 2007; **19**: 443–56. doi: https://doi.org/10.1016/j.clon.2007.03.014
2. Nathan P, Zweifel M, Padhani AR, Koh D-M, Ng M, Collins DJ, et al. Phase I trial of combretastatin A4 phosphate (CA4P) in combination with bevacizumab in patients with advanced cancer. *Clin Cancer Res* 2012; **18**: 3428–39. doi: https://doi.org/10.1158/1078-0432.CCR-11-3376
3. Shukla-Dave A, Obuchowski NA, Chenevert TL, Jambawalikar S, Schwartz LH, Malyarenko D, et al. Quantitative imaging biomarkers alliance (QIBA) recommendations for improved precision of DWI and DCE-MRI derived biomarkers in multicenter oncology trials. *J Magn Reson Imaging* 2019; **49**: e101–21. doi: https://doi.org/10.1002/jmri.26518
4. Leach MO, Morgan B, Tofts PS, Buckley DL, Huang W, Horsfield MA, et al. Imaging vascular function for early stage clinical trials using dynamic contrast-enhanced magnetic resonance imaging. *Eur Radiol* 2012; **22**: 1451–64. doi: https://doi.org/10.1007/s00330-012-2446-x
5. Port RE, Knopp MV, Brix G. Dynamic contrast-enhanced MRI using Gd-DTPA: interindividual variability of the arterial input function and consequences for the assessment of kinetics in tumors. *Magn Reson Med* 2001; **45**: 1030–8. doi: https://doi.org/10.1002/mrm.1137
6. Miyazaki K, Jerome NP, Collins DJ, Orton MR, d'Arcy JA, Wallace T, et al. Demonstration of the reproducibility of free-breathing diffusion-weighted MRI and dynamic contrast enhanced MRI in children with solid tumours: a pilot study. *Eur Radiol* 2015; **25**: 2641–50. doi: https://doi.org/10.1007/s00330-015-3666-7
7. Parker GJM, Roberts C, Macdonald A, Buonaccorsi GA, Cheung S, Buckley DL, et al. Experimentally-derived functional form for a population-averaged high-temporal-resolution arterial input function for dynamic contrast-enhanced MRI. *Magn Reson Med* 2006; **56**: 993–1000. doi: https://doi.org/10.1002/mrm.21066
8. Buckley DL. Uncertainty in the analysis of tracer kinetics using dynamic contrast-enhanced T1-weighted MRI. *Magn Reson Med* 2002; **47**: 601–6. doi: https://doi.org/10.1002/mrm.10080
9. Rata M, Collins DJ, Darcy J, Messiou C, Tunariu N, Desouza N, et al. Assessment of repeatability and treatment response in early phase clinical trials using DCE-MRI: comparison of parametric analysis using MR- and CT-derived arterial input functions. *Eur Radiol* 2016; **26**: 1991–8. doi: https://doi.org/10.1007/s00330-015-4012-9
10. Georgiou L, Wilson DJ, Sharma N, Perren TJ, Buckley DL. A functional form for a representative individual arterial input function measured from a population using high temporal resolution DCE MRI. *Magn Reson Med* 2019; **81**: 1955–63. doi: https://doi.org/10.1002/mrm.27524
11. Zöllner FG, Zimmer F, Klotz S, Hoeger S, Schad LR. Renal perfusion in acute kidney injury with DCE-MRI: deconvolution analysis versus two-compartment filtration model. *Magn Reson Imaging* 2014; **32**: 781–5. doi: https://doi.org/10.1016/j.mri.2014.02.014
12. Taouli B, Johnson RS, Hajdu CH, Oei MTH, Merad M, Yee H, et al. Hepatocellular carcinoma: perfusion quantification with dynamic contrast-enhanced MRI. *AJR Am J Roentgenol* 2013; **201**: 795–800. doi: https://doi.org/10.2214/AJR.12.9798
13. Lim SW, Chrysochou C, Buckley DL, Kalra PA, Sourbron SP. Prediction and assessment of responses to renal artery revascularization with dynamic contrast-enhanced magnetic resonance imaging: a pilot study. *Am J Physiol Renal Physiol* 2013; **305**: F672–8. doi: https://doi.org/10.1152/ajprenal.00007.2013
14. Jensen RL, Mumert ML, Gillespie DL, Kinney AY, Schabel MC, Salzman KL. Preoperative dynamic contrast-enhanced MRI correlates with molecular markers of hypoxia and vascularity in specific areas of intratumoral microenvironment and is predictive of patient outcome. *Neuro Oncol* 2014; **16**: 280–91. doi: https://doi.org/10.1093/neuonc/not148
15. Rajan S, Herbertson L, Bernardo M, Choyke P. A dialyzer-based flow system for validating dynamic contrast enhanced Mr image acquisition. *Magn Reson Med* 2014; **72**: 41–8. doi: https://doi.org/10.1002/mrm.24887
16. Kershaw LE, Cheng H-LM. A general dual-bolus approach for quantitative DCE-MRI. *Magn Reson Imaging* 2011; **29**: 160–6. doi: https://doi.org/10.1016/j.mri.2010.08.009
17. Risse F, Semmler W, Kauczor H-U, Fink C. Dual-bolus approach to quantitative measurement of pulmonary perfusion by contrast-enhanced MRI. *J Magn Reson Imaging* 2006; **24**: 1284–90. doi: https://doi.org/10.1002/jmri.20747
18. Fram EK, Herfkens RJ, Johnson GA, Glover GH, Karis JP, Shimakawa A, et al. Rapid calculation of T1 using variable FLIP angle gradient refocused imaging. *Magn Reson Imaging* 1987; **5**: 201–8. Accessed December 18, 2012. doi: https://doi.org/10.1016/0730-725X(87)90021-X
19. Haacke EM, Brown R, Thompson M, Venkatesan R. *Magnetic resonance imaging*. Chichester, UK: John Wiley & Sons Ltd; 2014.
20. Korporaal JG, van den Berg CAT, van Osch MJP, Groenendaal G, van Vulpen M, van der Heide UA. Phase-based arterial input function measurements in the femoral arteries for quantification of dynamic contrast-enhanced (DCE) MRI and comparison with DCE-CT. *Magn Reson Med* 2011; **66**: 1267–74. doi: https://doi.org/10.1002/mrm.22905
21. Cron GO, Foottit C, Yankeelov TE, Avruch LI, Schweitzer ME, Cameron I. Arterial input functions determined from Mr signal magnitude and phase for quantitative dynamic contrast-enhanced MRI in the human pelvis. *Magn Reson Med* 2011; **66**: 498–504. doi: https://doi.org/10.1002/mrm.22856
22. Foottit C, Cron GO, Hogan MJ, Nguyen TB, Cameron I. Determination of the venous

output function from Mr signal phase: feasibility for quantitative DCE-MRI in human brain. *Magn Reson Med* 2010; **63**: 772–81. doi: https://doi.org/10.1002/mrm.22253

23. Bleeker EJW, van Buchem MA, Webb AG, van Osch MJP. Phase-based arterial input function measurements for dynamic susceptibility contrast MRI. *Magn Reson Med* 2010; **64**: 358–68. doi: https://doi.org/10.1002/mrm.22420
24. Foltz W, Driscoll B, Laurence Lee S, Nayak K, Nallapareddy N, Fatemi A, Lee SL, et al. Phantom validation of DCE-MRI magnitude and phase-based vascular input function measurements. *Tomography* 2019; **5**: 77–89. doi: https://doi.org/10.18383/j.tom.2019.00001
25. Peeters F, Annet L, Hermoye L, Van Beers BE. Inflow correction of hepatic perfusion measurements using T1-weighted, fast gradient-echo, contrast-enhanced MRI. *Magn Reson Med* 2004; **51**: 710–7. doi: https://doi.org/10.1002/mrm.20032
26. Roberts C, Little R, Watson Y, Zhao S, Buckley DL, Parker GJM. The effect of blood inflow and B(1)-field inhomogeneity on measurement of the arterial input function in axial 3D spoiled gradient echo dynamic contrast-enhanced MRI. *Magn Reson Med* 2011; **65**: 108–19. doi: https://doi.org/10.1002/mrm.22593
27. van Schie JJN, Lavini C, van Vliet LJ, Vos FM. Estimating the arterial input function from dynamic contrast-enhanced MRI data with compensation for flow enhancement (I): theory, method, and phantom experiments. *J Magn Reson Imaging* 2018; **47**: 1190–6. doi: https://doi.org/10.1002/jmri.25906
28. Garpebring A, Wirestam R, Östlund N, Karlsson M. Effects of inflow and radiofrequency spoiling on the arterial input function in dynamic contrast-enhanced MRI: a combined phantom and simulation study. *Magn Reson Med* 2011; **65**: 1670–9. doi: https://doi.org/10.1002/mrm.22760
29. Han M, Hargreaves BA, a HB. Reduction of flow artifacts by using partial saturation in RF-spoiled gradient-echo imaging. *Magn Reson Med* 2011; **65**: 1326–34. doi: https://doi.org/10.1002/mrm.22729
30. Ning J, Schubert T, Johnson KM, Roldán-Alzate A, Chen H, Yuan C, et al. Vascular input function correction of inflow enhancement for improved pharmacokinetic modeling of liver DCE-MRI. *Magn Reson Med* 2018; **79**: 3093–102. doi: https://doi.org/10.1002/mrm.26988
31. Milnor WR. *Hemodynamics*. Baltimore: Williams and Wilkins; 1982.
32. Gwilliam MN, Hoggard N, Capener D, Singh P, Marzo A, Verma PK, et al. Mr derived volumetric flow rate waveforms at locations within the common carotid, internal carotid, and basilar arteries. *J Cereb Blood Flow Metab* 2009; **29**: 1975–82. doi: https://doi.org/10.1038/jcbfm.2009.176
33. Frayne R, Holdsworth DW, Gowman LM, Rickey DW, Drangova M, Fenster A, et al. Computer-Controlled flow simulator for Mr flow studies. *J Magn Reson Imaging* 1992; **2**: 605–12. doi: https://doi.org/10.1002/jmri.1880020522
34. Messiou C, Orton M, Ang JE, Collins DJ, Morgan VA, Mears D, et al. Advanced solid tumors treated with cediranib: comparison of dynamic contrast-enhanced MR imaging and CT as markers of vascular activity. *Radiology* 2012; **265**: 426–36. doi: https://doi.org/10.1148/radiol.12112565
35. Wang HZ, Riederer SJ, Lee JN. Optimizing the precision in T1 relaxation estimation using limited FLIP angles. *Magn Reson Med* 1987; **5**: 399–416. doi: https://doi.org/10.1002/mrm.1910050502
36. Imran J, Langevin F, Saint-Jalmes H. Two-Point method for T1 estimation with optimized gradient-echo sequence. *Magn Reson Imaging* 1999; **17**: 1347–56. doi: https://doi.org/10.1016/S0730-725X(99)00092-2
37. Venkatesan R, Lin W, Haacke EM. Accurate determination of spin-density and T1 in the presence of RF-field inhomogeneities and flip-angle miscalibration. *Magn Reson Med* 1998; **40**: 592–602. doi: https://doi.org/10.1002/mrm.1910400412
38. Zhang X, Petersen ET, Ghariq E, De Vis JB, Webb AG, Teeuwisse WM, et al. In vivo blood T(1) measurements at 1.5 T, 3 T, and 7 T. *Magn Reson Med* 2013; **70**: 1082–6. doi: https://doi.org/10.1002/mrm.24550
39. Sourbron SP, Buckley DL. On the scope and interpretation of the Tofts models for DCE-MRI. *Magn Reson Med* 2011; **66**: 735–45. doi: https://doi.org/10.1002/mrm.22861
40. Parker GJM, Barker GJ, Tofts PS. Accurate multislice gradient echoT1 measurement in the presence of non-ideal rf pulse shape and rf field nonuniformity. *Magn Reson Med* 2001; **45**: 838–45. doi: https://doi.org/10.1002/mrm.1112
41. Bryant DJ, Payne JA, Firmin DN, Longmore DB. Measurement of flow with NMR imaging using a gradient pulse and phase difference technique. *J Comput Assist Tomogr* 1984; **8**: 588–93. doi: https://doi.org/10.1097/00004728-198408000-00002
42. De Naeyer D, Verhulst J, Ceelen W, Segers P, De Deene Y, Verdonck P. Flip angle optimization for dynamic contrast-enhanced MRI-studies with spoiled gradient echo pulse sequences. *Phys Med Biol* 2011; **56**: 5373–95. doi: https://doi.org/10.1088/0031-9155/56/16/019
43. Schabel MC, Fluckiger JU, DiBella EVR. A model-constrained Monte Carlo method for blind arterial input function estimation in dynamic contrast-enhanced MRI: I. simulations. *Phys Med Biol* 2010; **55**: 4783–806. doi: https://doi.org/10.1088/0031-9155/55/16/011
44. Kholmovski EG, DiBella EVR. Perfusion MRI with radial acquisition for arterial input function assessment. *Magn Reson Med* 2007; **57**: 821–7. doi: https://doi.org/10.1002/mrm.21210